Dissociative Chemisorption of O_2 Inducing Stress Corrosion Cracking in Silicon Crystals

Anna Gleizer,[1] Giovanni Peralta,[2] James R. Kermode,[2] Alessandro De Vita,[2,3] and Dov Sherman[1]
[1]Department of Materials Science and Engineering, Technion, Haifa 32000, Israel
[2]Department of Physics, King's College London, Strand, London WC2R 2LS, United Kingdom
[3]CENMAT-UTS, Via Alfonso Valerio 2, 34127 Trieste, Italy
(Received 25 July 2013; published 18 March 2014

Fracture experiments to evaluate the cleavage energy of the $(110)[1\,\bar{1}\,0]$ and $(111)[1\,1\,\bar{2}]$ cleavage systems in silicon at room temperature and humidity give 2.7 ± 0.3 and 2.2 ± 0.2 J/m^2, respectively, lower than any previous measurement and inconsistent with density functional theory (DFT) surface energy calculations of 3.46 and 2.88 J/m^2. However, in an inert gas environment, we measure values of 3.5 ± 0.2 and 2.9 ± 0.2 J/m^2, consistent with DFT, that suggest a previously undetected stress corrosion cracking scenario for Si crack initiation in room conditions. This is fully confirmed by hybrid quantum-mechanics–molecular-mechanics calculations.

DOI: 10.1103/PhysRevLett.112.115501 PACS numbers: 62.20.mt, 62.20.mj, 71.15.Mb, 71.15.Pd

Brittle crystals are of primary importance to today's high tech industries, as they serve as the main building block for the microelectronics and optoelectronics industries, and a full understanding of fracture pathways would be extremely useful for the design of, for example, microelectromechanical systems with high resistance to fracture, preventing catastrophic failure in service [1]. Griffith [2], in his reversible thermodynamic theory for crack initiation in brittle solids, assumed that twice the relaxed free surface energy of a material 2γ is the material property that resists crack initiation; one needs only to evaluate the free surface energy of the material to predict crack initiation. Irwin [3] expanded the criterion by introducing Γ_0, the fracture energy, which includes a wider range of energy consumption mechanisms. For ideally brittle materials, $\Gamma_0 = 2\gamma$, while $\Gamma_0 > 2\gamma$ when other energy dissipation mechanisms are active. Whether Γ_0 significantly differs from 2γ in brittle crystals is still an open question.

Crack initiation originates with bond breaking events at the atomic scale [4]. The effect of environmental species on bond breaking mechanisms is a fundamental issue and is not yet fully understood: stress corrosion cracking, where cracks advance very slowly under subcritical loads under the concerted action of stress and chemistry, is well known in oxide glasses [5–7] but has not previously been thought to be important in covalent crystals such as silicon without polar bonds [8]. Silicon is, however, vulnerable to fatigue after cyclic loading [9] and can be cleaved by targeted stress corrosion reactions with implanted hydrogen in the SmartCut process [10], indicating it is not entirely immune to chemical fracture effects.

Researchers have debated the exact values of Γ_0 and 2γ for silicon crystals for over three decades. Fracture experiments with silicon crystals are limited. However, similar to what has previously been found for Si grain boundaries [11], the results show a large scatter, with $3.0 < \Gamma_0^{110} < 5.4$ J/m^2 for the (110) plane [12–16] and $2.5 < \Gamma_0^{111} < 5.0$ J/m^2 for the (111) plane [16–19]. Experimental measurements of the relaxed surface energy γ also show a large variation, with $2.8 < 2\gamma^{110}{}_{\text{expt}} < 3.8$ J/m^2 [20,21] and $2.3 < 2\gamma^{111}{}_{\text{expt}} < 5.0$ J/m^2 [20–23]. Calculations of relaxed surface energies using density functional theory (DFT) are in reasonable agreement with the measurements, yielding $3.40 < 2\gamma^{110}{}_{\text{DFT}} < 4.08$ J/m^2 and $2.72 < 2\gamma^{111}{}_{\text{DFT}} < 3.97$ J/m^2, depending on the surface reconstruction assumed and the approximation used for the exchange-correlation functional [24–26].

In an attempt to rationalize the large scatter of past experimental results, we have evaluated the cleavage energy of the $(110)[1\,\bar{1}\,0]$ and $(111)[1\,1\,\bar{2}]$ crack systems (using round brackets to denote the cleavage plane and square brackets to denote the crack propagation direction) of silicon using high-resolution fracture experiments: rectangular specimens with atomically sharp precracks cleaved under tension using the coefficient of thermal expansion mismatch method [Fig. 1; see also Ref. [27]]. The critical energy release rate at cleavage initiation (i.e., the cleavage energy) Γ_0 for each specimen was calculated with the ABAQUS finite element analysis code. The cleavage energy was first evaluated under standard temperature and pressure conditions.

We obtain systematically higher values of the cleavage energy whenever the precrack is not flat, offset [Fig. 1(b)], or tilted [Fig. 1(c)]. Because of this systematic bias, and in contrast to many materials properties, averaging does not decrease the uncertainty in Γ_0, instead leading to overestimates. The best estimate for the cleavage energy of a brittle crystal is therefore the minimum of all experimental results carried out under the same conditions, as this is the result with the closest to perfect correspondence in the position and direction of the water-quenched precrack and the propagating crack. In the $(110)[1\,\bar{1}\,0]$ crack system, misaligned or tilted cracks give rise to increased values of

the cleavage energy. Here, we see a smooth transition in the cleavage energy as a function of the extent of misalignment, which we can measure directly from the height of the step, visible in confocal optical and atomic force microscope images of the fracture surfaces [Figs. 1(b) and 1(c)].

Plotting the cleavage energy as a function of the step height [Fig. 2, blue (dark gray) circles] for specimens with parallel and straight precracks only, we find a remarkably low result for the minimally offset precrack of ~10 nm [Fig. 1(d)]: the cleavage energy at initiation for this crack system is $\Gamma_0 = 2.7 \pm 0.3$ J/m^2, which is the lowest value reported to date, actually low enough to lie distinctively below the range of experimental and calculated surface energies, indicating that subcritical crack initiation must be taking place. An example of poorly aligned precrack ($\Gamma_0 = 4 \pm 0.3$ J/m^2) is shown in Fig. 1(e).

Evaluating the cleavage energy of the $(111)[1\,1\,\bar{2}]$ system is more complex due to the strong tendency of these cracks to continue propagating on the original plane if the water-quenched precrack is offset with respect to the center line of the specimen (i.e., the plane of maximum K_I), consuming additional energy. For this system, we therefore report only fracture energies of the best aligned cracks with smooth fracture surfaces after initiation [Fig. 1(f)]. The cleavage energy at initiation for a precrack misaligned by 100 μm is 3.9 ± 0.2 J/m^2 [Fig. 1(g)] and becomes even higher for larger misalignment, while for very well-aligned precracks, we measured $\Gamma_0 = 2.2 \pm 0.2$ J/m^2 [Fig. 1(f) and Fig. 2, solid red (light gray) circles]. This is again the lowest cleavage energy obtained for this crack system.

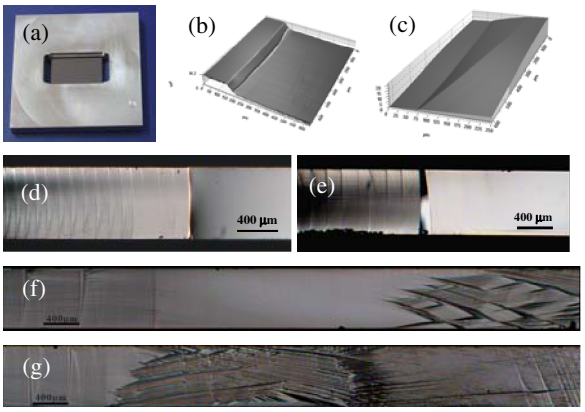

FIG. 1 (color online). Experimental fracture: (a) Optical photograph showing the assembly containing the Si specimen glued by epoxy resin to an aluminum loading frame. Confocal microscopy images showing examples of misalignment steps due to (b) offset or (c) tilted precracks. The effect of precrack or physical crack misalignment on the fracture surface of the $(110)[1\,\bar{1}\,0]$ system and the energy consumption in cleavage of silicon is demonstrated for well-aligned precrack, where (d) $\Gamma_0 = 2.7$ J/m^2, while for poorly aligned cracks, (e) $\Gamma_0 = 4$ J/m^2. For cracks initiating on the $(111)[1\,1\,\bar{2}]$ system: a well-aligned precrack, where (f) $\Gamma_0 = 2.2$ J/m^2 and a poorly aligned precrack (g) $\Gamma_0 = 3.9$ J/m^2.

The experiments were carried out at humidities of 20% and 55%, with no systematic dependence of the measured Γ_0 on humidity, suggesting that atmospheric oxygen rather than water is responsible for any chemically activated fracture processes (moreover, even at 55% humidity, there are at least 10 times more O_2 than H_2O molecules per unit volume). We also note that any liquid water droplet initially present in the cavity could not trail the crack along the $\gtrsim$50 μm long initiation region, as at our applied loads, the crack propagates faster than a stable droplet's maximum sustainable speed [28].

To investigate environmental effects on the fracture process, we remeasured the cleavage energy at initiation, this time placing the assembly in a vacuum chamber. At a vacuum of 10^{-3} Pa, the chamber was filled with 99.994% argon, and again the pressure was reduced to 10^{-3} Pa. This procedure was repeated five times. In the resulting inert gas environment, the cleavage energies for the $(110)[1\,\bar{1}\,0]$ and $(111)[1\,1\,\bar{2}]$ systems increased to $\Gamma_0 = 3.5 \pm 0.2$ and 2.9 ± 0.2 J/m^2, respectively [blue (dark gray) and red (light gray) solid squares in Fig. 2]. These larger values are in good agreement with the DFT calculations of 2γ of 3.46 and 2.88 J/m^2, respectively [24].

To explain the difference between the cleavage energies in standard and reduced oxygen conditions, we turn to molecular dynamics calculations of the dissociative chemisorption of oxygen molecules at crack tips. We performed hybrid quantum-mechanics–molecular-mechanics (QM-MM) fracture simulations using the "learn on the fly" (LOTF) scheme [29], first for the $(110)[1\,\bar{1}\,0]$ cleavage system. A large model system [$1200 \times 400 \times 5.43$ Å^3, with 129 794 atoms; Fig. 3] is needed to capture the effects of long-range

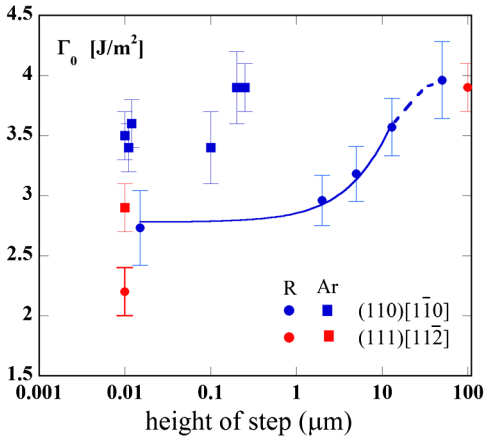

FIG. 2 (color online). The cleavage energy Γ_0 vs parallel and straight misalignment step height for $(110)[1\,\bar{1}\,0]$ [blue (dark gray) marks] and $(111)[1\,1\,\bar{2}]$ [red (light gray) marks] crack systems of silicon under room conditions (solid circles, labeled R) and atmospheric pressure of Ar (solid squares, Ar). The error of Γ_0 was defined by the error in temperature measurements of ± 0.1 °C during cleavage, which was used by ABAQUS to evaluate the range of the Γ_0.

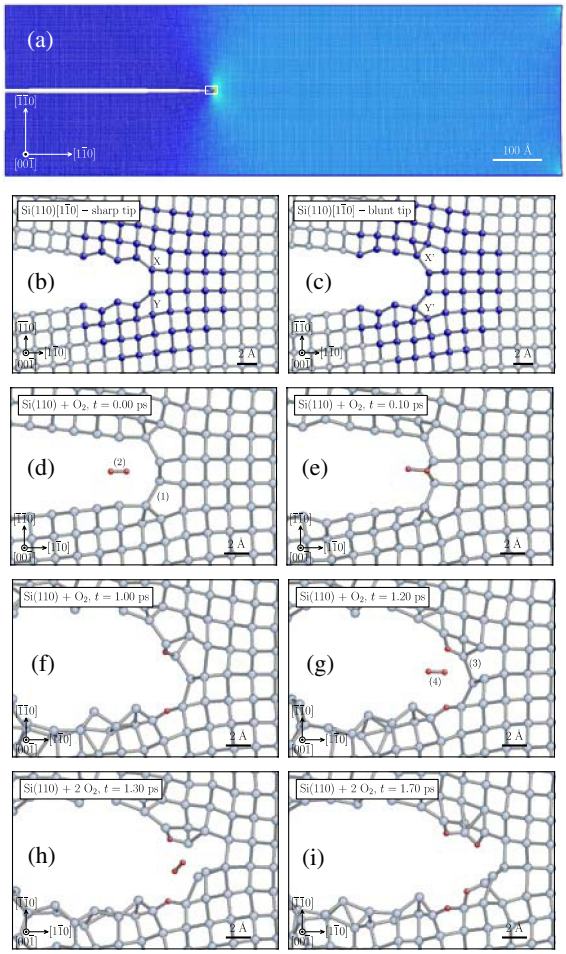

FIG. 3 (color online). Stress corrosion cracking in the Si(110)[1 $\bar{1}$ 0] cleavage system. (a) Model system, colored by principal stress, with red (light gray) regions corresponding to high tensile stress and dark blue (dark gray) regions to zero; the black rectangle shows the region shown in subsequent panels. Crack tip structures obtained by QM-MM geometry optimization with (b) a sharp crack tip and (c) a lower energy blunt crack tip, related to the sharp tip by rotation of bonds X/X' and Y/Y'. Dark blue (dark gray) atoms are treated at the QM level. (d)–(i) Snapshots from QM-MM dynamics showing dissociative chemisorption of two O_2 molecules and the resulting crack advance (see the text). Bonds shown are based on time-averaged atomic positions.

elastic relaxation [30]. To describe crack tip chemistry correctly, around 200 atoms near the crack tip were selected for quantum mechanical treatment at the DFT level [31], using the generalized gradient approximation to the exchange-correlation potential [32] as implemented in the VASP [33] and CASTEP [34] codes. A subcritical tensile load equivalent to an energy release rate of $G = 2.7$ J/m^2 was applied by rigidly clamping the top and bottom edges [35].

To identify the starting point for dynamical simulations, we performed a hybrid QM-MM relaxation of the full crack system [36], leading to a novel tip structure with a slightly blunted tip, formed from the sharp tip by two bond rotations [Figs. 3(b) and 3(c); cf. 5–7 tip reconstruction in Ref. [30]]. We find that the local chemical cost of the bond rotations is compensated by a reduction in elastic energy: the blunted tip system is lower in energy by 0.12 eV per unit crack front, suggesting it is the preferred equilibrium crack tip structure.

LOTF molecular dynamics simulations at a temperature of 300 K confirm that at $G = 2.7$ J/m^2, the crack neither advances nor closes up, remaining pinned by the lattice trapping barrier [37,38]. We then placed an oxygen molecule 4.0 Å behind the first unbroken Si-Si bond of the relaxed crack tip configuration [Fig. 3(d)] and restarted the simulation. The chemisorption energy of an O_2 molecule on a unstressed, reconstructed silicon surface is of the order of 5 eV [39], with an activation barrier of 0.2–0.3 eV [40]. Here, we observe immediate spontaneous dissociation of the oxygen molecule [Figs. 3(e) and 3(f)], indicating that dissociation becomes barrierless under these conditions [the enhanced O_2 approaching speed observed at small O_2-tip distances is also consistent with an independently calculated DFT adsorption energy profile constrained to the molecule orientation of Fig. 3(d)]. The oxygen is adsorbed to form Si-O-Si bridges behind the crack tip [Fig. 3(f)], leading to crack advance via cleavage of the Si-Si bond [labeled (1) in Fig. 3(d)]. The simulation was continued by adding a second O_2 molecule, which undergoes a similar pattern of dissociative chemisorption, Si-O-Si bridge formation, and crack advance [Figs. 3(g)–3(i)].

Moving to the (111) cleavage plane, we carried out LOTF simulations in a Si(111)[1 1 $\bar{2}$] model system (dimensions $1200 \times 400 \times 3.84$ Å^3, with 90 730 atoms; see Fig. 4). The crack surface behind the tip was saturated with hydrogen to reduce the number of possible O_2 reaction

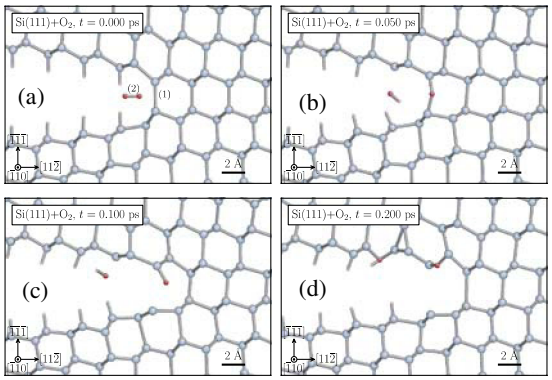

FIG. 4 (color online). Stress corrosion cracking in the Si(111)[1 1 $\bar{2}$] fracture system. As in Fig. 3, panels show only the near tip region, treated with QM accuracy. An O_2 molecule [red (dark gray) spheres] inserted 1.5 Å behind the crack tip (a) immediately dissociates, (b) in this case, forming an OH^- radical, and (c) subsequently chemisorbs, leading to crack advance via cleavage of the Si-Si bond labeled (1) at the crack tip. (d) After 0.2 ps, both oxygen atoms are incorporated in stable Si-O-Si bridges.

sites, allowing the delivery to the crack tip of the molecules inserted in the course of the simulation, avoiding spurious chemisorption on the fracture surfaces, not likely in the earlier $(110)[1\,\bar{1}\,0]$ crack systems because of the more open geometry of its crack tip [cf. Fig. 3(c); in the experimental system, the fracture surfaces are expected to be fully passivated with a native oxide layer [41]]. We again observe immediate dissociative chemisorption of oxygen [Fig. 4(b)] at the crack tip followed by Si-Si bond cleavage [Fig. 4(c)], leading to crack advance [Fig. 4(d)] at subcritical energy release rates as low as $G = 2.2\ \mathrm{J/m^2}$.

In a number of simulations in both the (110) and (111) systems, we see that the dissociation of a single O_2 molecule provides sufficient heat to "burn" at most one Si-Si bond at the crack tip. At least one oxygen molecule is required for each crack advance step. The heat locally released by the exothermic dissociative chemisorption is efficiently dissipated into the crystal matrix and never observed to cause the breaking of Si-Si bonds not directly bonding with an O atom to yield multiple advance steps. We note that such a physical effect would be favored by the periodic boundary conditions we use along the crack front, which correspond to an infinite row of molecules simultaneously approaching the crack tip. We conclude that slow fracture can be initiated at subcritical loads, with the crack advancing by stress corrosion through iterated oxidation or bond breaking steps occurring at the tip before any thick oxide layer has a chance to form.

The long-range elastic effect of the chemical reactions taking place at the crack tip can be measured by fitting the time-averaged atomistic stress field, calculated for each atom from its deformation relative to the perfect crystal [42], to the Irwin near-field solution for a sharp crack [3]. The fit was performed in an annular region extending from 5 to 100 Å from the geometrical tip, allowing the origin of the stress field to vary to minimize the difference between atomistic and continuum stress fields. For the (111) system, illustrated in Fig. 5(a), we see that following the dissociation and chemisorption of the O_2 molecule [O-O distance increasing, red (light gray) line], the crack advances by $a \sim 3$ Å unit step in the $[1\,1\,\bar{2}]$ crack propagation direction (green line). The Si-Si bond at the crack tip [blue (dark gray) line] ruptures concurrently with the advance of the stress field. This advance is irreversible due to the bond termination ("corking") effect of the adsorbed oxygen. The interplay between individual bond breaking events and the long-range elastic behavior is more complex in the (110) system [Fig. 5(b)], as the slight blunting of the tip allows a number of distinct reaction pathways. The first O_2 molecule illustrated in Fig. 3 dissociates immediately, eventually leading to the formation of two Si-O-Si bridges. By the time these bridges have fully formed, they are already effectively unloaded, as the center of the crack tip stress field [green line in Fig. 5(b)] advances very soon after the dissociation of the molecule, leading later to the breaking of

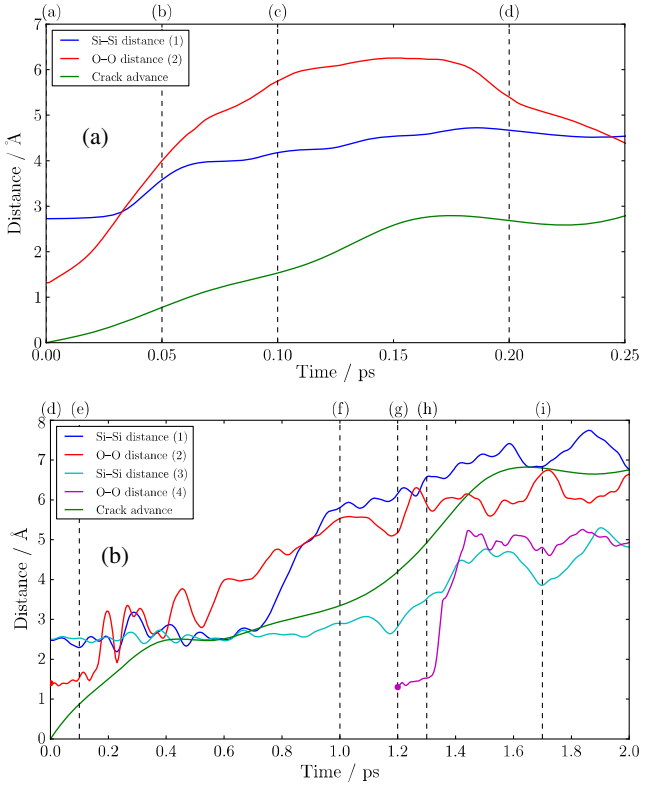

FIG. 5 (color online). Analysis of bond breaking and stress concentration in the (a) Si(111) and (b) Si(110) cleavage systems. Red (light gray) and magenta (mid dark gray) lines: O-O distances, increasing during dissociation. Blue (very dark gray) and cyan (very light gray) lines: Si-Si bonds cleaved during crack advance. Green (mid gray) lines: horizontal crack advance, measured by fitting the atom-resolved stress field to the Irwin near-field solution. Advance of the stress field can occur either (a) at the same time as or (b) before Si-Si bond rupture (see the text). Vertical dashed lines correspond to the labeled snapshots illustrated in Figs. 3 and 4.

the Si-Si bond labeled (1) in Fig. 3(d), in what could be interpreted as a localized toughening response. The adsorption of the second O_2 molecule [labeled (4) in Fig. 3(g)] leads, however, to perfectly brittle crack advance, with dissociation and absorption preceding the immediate rupture of the Si-Si bond [labeled (3) in Fig. 3(g)].

In summary, we find that oxygen molecules play the role of a corrosive agent capable of initiating fracture at subcritical loads on the Si(111) and Si(110) cleavage planes, contrary to the common wisdom in Si. In both experiments and atomistic simulations, cracks in an argon atmosphere do not propagate at energy release rates below the Griffith critical value of twice the surface energy density. The presence of an oxygen-rich environment leads to subcritical crack growth, revealed for the first time by our experiments in vanishing misalignment conditions. This is consistent with the dissociative chemisorption of O_2 molecules followed by cleavage of individual, stressed Si-Si bonds at the crack tip observed in our simulations. We

note that, in this barrierless dissociation regime, the speed of the subsequent crack growth will be limited by the time taken for oxygen to diffuse to the crack tip [43], so here we have focused on crack initiation, leaving a full discussion of the influence of the complex rheology of confined fluids on fracture propagation for a future work.

J. R. K. and A. D. V. acknowledge funding from the Rio Tinto Centre for Advanced Mineral Recovery based at Imperial College, London, and useful discussions with Gert van Hout and Jan Cilliers throughout the project. A. D. V. acknowledges funding from the EPSRC HEmS Grant No. EP/L014742/1. G. P., J. R. K., A. D. V., and D. S. acknowledge funding from the European Commission ADGLASS FP7 project. This research used resources of the Argonne Leadership Computing Facility at Argonne National Laboratory, which is supported by the Office of Science of the U.S. Department of Energy under contract DE-AC02-06CH11357. The authors thank Matteo Ciccotti for useful discussions.

[1] S. M. Spearing, Acta Mater. **48**, 179 (2000).
[2] A. A. Griffith, Phil. Trans. R. Soc. A **221**, 163 (1921).
[3] G. R. Irwin, *Fracturing of Metals* (American Society for Metals, Cleveland, 1948), p. 147.
[4] B. R. Lawn, *Fracture of Brittle Solids*(Cambridge University Press, Cambridge, England, 1993), 2nd ed.
[5] S. Wiederhorn, J. Am. Ceram. Soc. **50**, 407 (1967).
[6] T. A. Michalske and S. W. Freiman, Nature (London) **295**, 511 (1982).
[7] M. Ciccotti, J. Phys. D **42**, 214006 (2009).
[8] R. F. Cook, J. Mater. Sci. **41**, 841 (2006).
[9] J. A. Connally and S. B. Brown, Science **256**, 1537 (1992).
[10] G. Moras, L. Ciacchi, C. Elsässer, P. Gumbsch, and A. De Vita, Phys. Rev. Lett. **105**, 075502 (2010).
[11] J. Zhang, C.-Z. Wang, and K.-M. Ho, Phys. Rev. B **80**, 174102 (2009).
[12] R. J. Jaccodine, J. Electrochem. Soc. **110**, 524 (1963).
[13] S. Bhaduri and F. Wang, J. Mater. Sci. **21**, 2489 (1986).
[14] G. Michot, Cryst. Prop. Prep. **17-18**, 55 (1988).
[15] F. Ebrahimi and L. Kalwani, Mater. Sci. Eng. A **268**, 116 (1999).
[16] C. Chen and M. Leipold, Am. Ceram. Soc. Bull. **59**, 469 (1980).
[17] B. Lawn, D. Marshall, and P. Chantikul, J. Mater. Sci. **16**, 1769 (1981).
[18] J. A. Hauch, D. Holland, M. P. Marder, and H. L. Swinney, Phys. Rev. Lett. **82**, 3823 (1999).
[19] T. Cramer, A. Wanner, and P. Gumbsch, Phys. Rev. Lett. **85**, 788 (2000).
[20] C. Messmer and J. Bilello, J. Appl. Phys. **52**, 4623 (1981).
[21] D. J. Eaglesham, A. E. White, L. C. Feldman, N. Moriya, and D. C. Jacobson, Phys. Rev. Lett. **70**, 1643 (1993).
[22] J. J. Gilman, J. Appl. Phys. **31**, 2208 (1960).
[23] C. St John, Philos. Mag. **32**, 1193 (1975).
[24] R. Perez and P. Gumbsch, Phys. Rev. Lett. **84**, 5347 (2000).
[25] A. A. Stekolnikov, J. Furthmüller, and F. Bechstedt, Phys. Rev. B **65**, 115318 (2002).
[26] G.-H. Lu, M. Huang, M. Cuma, and F. Liu, Surf. Sci. **588**, 61 (2005).
[27] A. Gleizer and D. Sherman (unpublished).
[28] A. Grimaldi, M. George, G. Pallares, C. Marliére, and M. Ciccotti, Phys. Rev. Lett. **100**, 165505 (2008).
[29] G. Csányi, T. Albaret, M. C. Payne, and A. De Vita, Phys. Rev. Lett. **93**, 175503 (2004).
[30] J. R. Kermode, T. Albaret, D. Sherman, N. Bernstein, P. Gumbsch, M. C. Payne, G. Csányi, and A. De Vita, Nature (London) **455**, 1224 (2008).
[31] W. Kohn and L. J. Sham, Phys. Rev. **140**, A1133 (1965).
[32] J. P. Perdew, K. Burke, and M. Ernzerhof, Phys. Rev. Lett. **77**, 3865 (1996).
[33] G. Kresse and J. Furthmüller, Phys. Rev. B **54**, 11169 (1996).
[34] S. J. Clark, M. D. Segall, C. J. Pickard, P. J. Hasnip, M. I. J. Probert, K. Refson, and M. C. Payne, Z. Kristallogr. **220**, 567 (2005).
[35] J. G. Swadener, M. I. Baskes, and M. Nastasi, Phys. Rev. Lett. **89**, 085503 (2002).
[36] E. Bitzek, P. Koskinen, F. Gahler, M. Moseler, and P. Gumbsch, Phys. Rev. Lett. **97**, 170201 (2006).
[37] R. Thomson, C. Hsieh, and V. Rana, J. Appl. Phys. **42**, 3154 (1971).
[38] N. Bernstein and D. W. Hess, Phys. Rev. Lett. **91**, 025501 (2003).
[39] K. Kato and T. Uda, Phys. Rev. B **62**, 15 978 (2000).
[40] U. Höfer, P. Morgen, W. Wurth, and E. Umbach, Phys. Rev. B **40**, 1130 (1989).
[41] L. Colombi Ciacchi, D. J. Cole, M. C. Payne, and P. Gumbsch, J. Phys. Chem. C **112**, 12 077 (2008).
[42] G. Moras, R. Choudhury, J. R. Kermode, G. Csányi, M. C. Payne, and A. De Vita, in *Trends in Computational Nanomechanics: Transcending Length and Time Scales*, edited by T. Dumitrica (Springer, New York, 2010), p. 1.
[43] B. R. Lawn, Mater. Sci. Eng. **13**, 277 (1974).